Robotics and Autonomous Systems 100 (2018) 150–159

Contents lists available at ScienceDirect

Robotics and Autonomous Systems

journal homepage: www.elsevier.com/locate/robot

Position/force operational space control for underwater manipulation

Corina Barbalata [a,*,1], Matthew W. Dunnigan [b], Yvan Petillot [b]

[a] Naval Architecture and Marine Engineering, University of Michigan, Ann Arbor, USA
[b] School of Engineering and Physical Sciences, Heriot-Watt University, Edinburgh, UK

HIGHLIGHTS

- A position/force control architecture is designed for an underwater manipulator.
- The control law handles approximated contact forces with the environment in the case when a force sensor is not available.
- Incorporating an estimate of the dynamic model and the theory of sliding mode theory leads to a robust and stable behaviour.
- A valid alternative to the Impedance Control, handling some of the challenges present in the Impedance control.
- Experimental results prove the validity of the system.

ARTICLE INFO

Article history:
Received 4 July 2017
Received in revised form 19 October 2017
Accepted 14 November 2017
Available online 2 December 2017

Keywords:
Underwater manipulation
Control
Task space
Model based
Robust control
Hybrid control

ABSTRACT

An underwater manipulator is a complex system, highly non-linear and subject to disturbances caused by underwater effects. To obtain a reliable system, robust control strategies have to be designed for the manipulator. The main contribution of this paper is the development of the low-level position/force control structure for an underwater manipulator. The proposed control strategy is planned in the operational space and combines together the parallel control structure for position/force applications with the sliding mode theory and the manipulator model information. The dynamic model of the system incorporates the hydrodynamic effects and an approximation of the end-effector force contact with the environment. This paper presents a method for computing the interaction force at the end-effector in the absence of a force–torque sensor. The control structure is validated through a Lyapunov-stability approach and experimental results. The control structure is tested on a 6 degrees-of-freedom underwater manipulator interacting with the underwater environment.

1. Introduction

The inspection and surveillance of the oceans is increasingly performed with autonomous vehicles for the oil and gas industry, military applications and various research applications. These systems are commercially available and there is a constant desire to improve them. Therefore, scientists are interested in extending the autonomy of the robots to interact with the underwater environment. An underwater manipulator placed on a mobile platform is subject to a large number of disturbances such as hydrodynamic effects, sea currents, disturbances caused by the movement of the mobile base and/or large contact forces caused by interaction with the environment.

The underwater manipulation tasks are naturally defined in the operational space while the control actions have to be represented at joint level. Nevertheless, the control structure for underwater manipulators can be designed either in the joint space or in the operational space and further projected to joint space. The advantage of the operational space controllers rests in the fact that the task error is directly minimised by the feedback loop [1].

The operational space control structure is presented in [2] for vehicle and arm coordination as well as for multiple manipulators working together. The experimental results shows the validity of designing the control law in the operational space for the case when multibody systems have to be used to perform the specified tasks. Other control schemes developed in end-effector coordinates for underwater manipulators have been proposed recently in [3,4]. The manipulators are part of vehicle-manipulator systems where the control schemes are designed to handle environmental disturbances and perform accurate end-effector trajectory tracking. The redundancy exploitation of the UVMS is a key factor in solving the task control problem in [5] and [6]. Underwater

* Corresponding author.
E-mail addresses: corinaba@umich.edu (C. Barbalata), m.w.dunnigan@hw.ac.uk (M.W. Dunnigan), y.r.petillot@hw.ac.uk (Y. Petillot).
[1] During this work the author was with the School of Engineering and Physical Sciences, Heriot-Watt University, Edinburgh, UK.

https://doi.org/10.1016/j.robot.2017.11.004
0921-8890/

manipulation tasks are controlled through an operational space fuzzy controller in [7]. The authors demonstrate through the simulation results that the proposed strategy can track the desired end-effector position and provides robust performance. The design of the control structure in the workspace is realised in [8] where a complete low-level/high-level control structure is presented for a free-floating manipulator.

A compliant control structure for underwater manipulation is proposed in [9] for applications where the system has to interact with the environment. The paper is focused on the design of the manipulator and the authors state that impedance controllers can be used for force control applications with this manipulator. The control structure for a hydraulic underwater manipulator is presented in [10]. The authors demonstrate the validity of the hybrid position/force control structure for a manipulator with a force sensor through experimental results. The force at the end-effector is directly controlled for underwater manipulation in [11]. The author proposes two direct control schemes for interaction with the environment. In the first control strategy the force error is directly incorporated in the control command from the motion controller. In this case the motion controller is represented through a PID law. In the second control strategy the force error is incorporated in the velocity control law of the system. The output of this control law is further incorporated into the motion controller represented through a sliding mode regulator. The simulation results show that both controllers are robust to uncertainties in the system, hydrodynamic effects and poor performance of the vehicle controller. The control of both position and force for underwater manipulation is presented in [12]. The control system combines the hybrid structure with an impedance controller. The impedance controller is used up to the point where interaction with the environment takes place to ensure a soft contact with the environment. From this point onwards, this control structure is replaced by the hybrid control to ensure the desired interaction force is maintained. A parallel force/position controller is used in [13] for the control of an underwater manipulator placed on an autonomous vehicle. A model free control law is used as the position control structure and through simulation results it is shown that the controller is robust to external disturbances and fulfils the system requirements.

For underwater environments the model based control structures represent one of the main approaches used in the literature for handling the environmental disturbances. These types of controllers can be used to linearise the system and to describe a coupled control architecture for a floating base and manipulator as presented in [14]. In [15] a model based controller is proposed for a 3 degrees-of-freedom (DOF) underwater manipulator. A sliding mode controller is developed for a trajectory tracking application. The sliding mode controller (SMC) represents a robust approach that is able to handle the uncertainties and disturbances from the underwater effects. It has been used for motion tracking control in underwater environments in [16], together with a fuzzy-component for the gain tuning. Based on simulation results the authors conclude that the proposed tuning improves the performances of the SMC controller. A similar approach is presented in [17] where a SMC with fuzzy tuning is implemented for an underwater-vehicle manipulator system. The performance of the system is validated through simulation results with a 5-DOF UVMS for trajectory tracking applications. Through experimental results a SMC controller is evaluated in [18]. The controller is implemented on an underwater three fingered gripper.

The main goal of this paper is to present a novel low-level control structure for an underwater manipulator for applications including trajectory tracking and interaction with the surrounding environment. The novelty of the paper rests in the structure of the controller. Although the sliding mode control law is a well studied approach, it is incorporated into a parallel position/force control strategy for the first time. Previous work in the field either incorporated the control law in a hybrid position/force control law [19,20] or in an impedance approach [21,22]. The main strength of the proposed law is shown through experimental results and consists in the fact that the method handles approximated contact forces with the environment, when a force sensor is not available. Furthermore uncertainties in the system and disturbances created by the contact with the environment are handled by a novel way of incorporating an estimate of the dynamic model with the sliding mode theory.

A model based structure is used in the control law based on the mathematical representation of the system presented in Section 2. The overall control structure using the parallel position/force strategy and a variable structure law is described in Section 3. The experimental set-up used to evaluate the control law is described in Section 4 and the results are presented in Section 5. A few comments on the experimental results are presented in Section 6 followed by the conclusions of the paper in Section 7.

2. Mathematical model

The closed form mathematical model of an underwater manipulator interacting with the environment is represented through Eq. (1).

$$M(\rho)\ddot{\rho} + C(\rho, \dot{\rho})\dot{\rho} + D(\rho, \dot{\rho})\dot{\rho} + g(\rho) + f_f(\rho) = \tau - J^{-1}F \tag{1}$$

where $\rho \in \mathbb{R}^n$ are the joint positions, $\dot{\rho} \in \mathbb{R}^n$ are the joint velocities and $\ddot{\rho} \in \mathbb{R}^n$ are the joint accelerations. $M(\rho) \in \mathbb{R}^{n\times n}$ is the inertia matrix, $C(\rho, \dot{\rho})\dot{\rho} \in \mathbb{R}^n$ is the Coriolis and Centripetal matrix, $D(\rho, \dot{\rho})\dot{\rho} \in \mathbb{R}^n$ is the hydrodynamic drag, $g(\rho) \in \mathbb{R}^n$ is the restoring forces vector, $f_f \in \mathbb{R}^n$ is the friction of the system, $F \in \mathbb{R}^6$ is the vector of interaction forces with the environment and $\tau \in \mathbb{R}^n$ is the vector of generalised forces applied to the manipulator, $J \in \mathbb{R}^{6\times n}$ is the manipulator Jacobian and n is the number of degrees-of-freedom of the manipulator.

The mathematical model is obtained by approximating each link as a cylinder and applying the laws of physics. A recursive implementation is used to compute the overall model, based on the Composite Rigid Body Algorithm [23], the Newton–Euler Algorithm and incorporating the hydrodynamic effects.

$M(\rho)$ is interpreted as the matrix of forces that distributes an acceleration on a stationary system. Each column of the $M(\rho)$ matrix is interpreted as the vector of forces to produce a unit acceleration onto the corresponding link. To compute the values of the column i, it is considered that the links from i to the last link are moving, while the previous links are static. Based on this assumption every joint transmits a force, defined based on the inertial components, onto the subsequent link. The matrix $M(\rho)$ is computed according to:

$$M(\rho) = \begin{bmatrix} M_{11} & \cdots & M_{1n} \\ & \ddots & \\ M_{n1} & \cdots & M_{nn} \end{bmatrix} \tag{2}$$

where

$$M_{ij} = \begin{cases} s_i^T I_i^c s_j & \text{if } i \in \lambda(j) \\ s_i^T I_j^c s_j & \text{if } j \in \lambda(i) \\ 0 & \text{otherwise} \end{cases} \tag{3}$$

where $\lambda(j)$ represents the set of parents for joint j and I_i^c is the inertia of the subtree that starts at the rigid body i. The inertia is computed based on the sum of inertias of all links that are part of the subtree:

$$I_i^c = I_i + \sum_{j\in\mu(i)} I_j^c \tag{4}$$

where $\mu(i)$ is the set of the children of joint i.

The Coriolis force is computed in the direction perpendicular to the rotation axis, proportional to the angular rigid body velocity and the centrifugal force acts outwards in the radial direction being computed based on the distance of the rigid body from the rotating frame [24]. To compute the Coriolis and centripetal forces $C(\dot{\rho}, \rho)\dot{\rho}$ the inverse dynamics methodology is used. According to [23] in this case the acceleration is considered to be $\ddot{q} = 0$ and the desired information is the force that acts on the system. The recursive Newton–Euler algorithm represents one of the most popular and simple solutions to solve this problem. In the first step the velocity and acceleration of the ith rigid body is computed by Eq. (5) and Eq. (6). Applying recursively these equations from the first to the last degree-of-freedom computes the velocity and acceleration for every rigid body in the system.

$$v_i = v_{\lambda(i)} + s_i\dot{\rho}_i, \quad v_0 = 0 \tag{5}$$

$$a_i = a_{\lambda(i)} + s_i\ddot{\rho}_i + \dot{s}_i\dot{\rho}_i, \quad a_0 = 0 \tag{6}$$

where v_i represents the velocity of the body i, a_i is the acceleration of body i, $v_{\lambda(i)}$ and $a_{\lambda(i)}$ the velocity and acceleration of the parent of the body i, s_i represents the allowed movement of the joint, $\ddot{\rho}_i$, $\dot{\rho}_i$ are the acceleration and velocity of the generalised degree-of-freedom i. The net force f_i^b applied on the ith rigid body, dependent on the joint acceleration and velocity, is represented by Eq. (7) and it is computed based on the inertial value of the current component I_i.

$$f_i^b = I_i a_i + v_i \times I_i v_i \tag{7}$$

The force transmitted from the parent body $\lambda(i)$ across joint i is marked as f_i and it is described by Eq. (8) and depends on the force applied on the current link f_i^b, the force f_j in the set of children of the body i, $\mu(i)$ and external forces f_i^x. The external forces can be caused by the added mass forces.

$$\begin{aligned} f_i^b &= f_i + f_i^x - \sum_{j\in\mu(i)} f_j \\ f_i &= f_i^b - f_i^x + \sum_{j\in\mu(i)} f_j \end{aligned} \tag{8}$$

In this work the added mass forces and moments consist of inertia force and moments and the Coriolis and centripetal force and moments. Considering unbounded fluid with irrational flow and low values of viscosity, Newman [25] presents in his work a set of equations that compute the added mass force acting on an accelerating rigid body. The equations connect the acceleration of the body with the added mass inertia matrix (also named added mass coefficients), as presented in:

$$f_i^x = I_{a_i} a_i + v_i \times I_{a_i} v_i \tag{9}$$

where I_{a_i} is the added mass inertia matrix component.

The $C(\dot{\rho}, \rho)\dot{\rho}$ vector is the vector of all the generalised forces at the joints, as given by:

$$C(\dot{\rho}, \rho)\dot{\rho} = \left[s_1^T f_1,\ s_2^T f_2, \ldots, s_n^T f_n\right]^T \tag{10}$$

To obtain the drag force the moment integral along the length of the cylinder has to be performed as presented in:

$$D(\dot{\rho}, \rho)\dot{\rho} = -\rho_w C_D r \int_0^l \|v\| v dx \tag{11}$$

where $C_D \in \mathbb{R}$ is the drag coefficient, $l \in \mathbb{N}$ is the length of the link, $r \in \mathbb{N}$ is the radius of the link and $v \in \mathbb{R}$ is the velocity relative to the fluid and normal to the edge of each disc. The drag component in the direction of the cylinder axis can be computed based on, [26]:

$$D(\dot{\rho}, \rho)\dot{\rho} = -0.5\rho_w C_D \pi r^2 \|v\| v \tag{12}$$

The buoyancy force is proportional to the mass of the fluid displaced by the moving body. It is exerted opposite to the gravitational force, as presented by Archimedes principle, Eq. (13).

$$f_b = -m_d a_g = -\rho_w V a_g \tag{13}$$

where $m_d \in \mathbb{N}$ is the mass of the fluid displaced, $V \in \mathbb{N}$ is the volume displaced and $a_g = 9.8\ \mathrm{m/s^2}$ is the gravitational acceleration. The restoring force can be described by Eq. (14), where $m \in \mathbb{N}$ represents the mass of the rigid body.

$$g(\rho) = m a_g + f_b \tag{14}$$

The friction model used in this work is:

$$f_f = c\dot{\rho} \tag{15}$$

where $c \in \mathbb{R}^+$ represents the viscous coefficient.

The mathematical representation of the system in operational space is described by Eq. (16), [27].

$$M(x)\ddot{x} + C(x)\dot{x} + D(x)\dot{x} + G(x) + F_f(x) = T - F \tag{16}$$

where $x \in \mathbb{R}^6$ is the position vector described in the operational space, $M(x) \in \mathbb{R}^{6\times6}$ is a positive operational space inertia matrix, $C(x)\dot{x} \in \mathbb{R}^6$ is the vector of Coriolis and Centripetal forces, $D(x)\dot{x} \in \mathbb{R}^6$ is the drag vector, $G(x) \in \mathbb{R}^6$ is the vector of restoring forces, $F_f(x) \in \mathbb{R}^6$ is the friction vector, all defined in operational space coordinates, $T \in \mathbb{R}^6$ is the vector of generalised forces at the end-effector and $F \in \mathbb{R}^6$ is the vector of contact forces at the end-effector. The dynamic components in the operational space are defined with respect to the system coordinates by the following equations as presented in [28]:

$$\begin{aligned} M(x) &= \left(JM^{-1}(\rho)J^T\right)^{-1} \\ C(x) &= \bar{J}^T C(\rho, \xi) - M(x)\dot{J}\dot{\rho} \\ D(x) &= \bar{J}^T D(\rho, \xi) - M(x)\dot{J}\dot{\rho} \\ G(x) &= \bar{J}^T g(\rho) \\ \bar{J}^T &= M^{-1}(q)J^T M(x) \end{aligned} \tag{17}$$

where $\bar{J}^T$ is the dynamically consistent generalised inverse of the Jacobian. In the case an invertible Jacobian, the following relation holds $\bar{J}^T = J^{-1}$.

The interaction force at the end-effector can be measured with a force sensor or approximated based on joint information when a sensor is not available. In [29] the contact force is approximated based on the joint torques. This approach is developed further including a recursive least-squares algorithm to estimate the force in [30] and a disturbance observer component is used in [31] to estimate the contact force.

For the system used in this study a force sensor is not available and the contact force is estimated using the mathematical model of the robot and considering the torque–current relationship. The force vector F is mapped to the joint torque using Eq. (18).

$$\tau_f = J^T(\rho)F \tag{18}$$

This leads to the estimate of the end-effector contact forces and torques:

$$F = \left(J^T(\rho)\right)^{\dagger}\tau_f \tag{19}$$

where $\left(J^T(\rho)\right)^{\dagger}$ is the pseudo-inverse of the Jacobian transpose. The total torque at joint level, τ, is described based on Eq. (20):

$$\tau = \tau_p - \tau_f \tag{20}$$

where $\tau_p \in \mathbb{R}^n$ is the torque needed to produce a certain motion or maintain a position and $\tau_f \in \mathbb{R}^n$ is the torque produced by the

contact with the environment. The motion related torques can be estimated using the mathematical model of the robot as presented in Eq. (21).

$$\tau_p = M(\rho)\ddot{\rho} + C(\rho, \dot{\rho})\dot{\rho} + D(\rho, \dot{\rho})\dot{\rho} + g(\rho) \tag{21}$$

where $\ddot{\rho}$, $\dot{\rho}$ and ρ are obtained based on measurements from the robot. For the manipulator used in this study, at each joint there is a DC permanent magnet motor with current measurements available. The total torque at each joint is approximated using Eq. (22).

$$\tau = k_\tau^T i_a \tag{22}$$

where $k_\tau \in \mathbb{R}^n$ is the vector of torque constants and $i_a \in \mathbb{R}^n$ is the vector of motor armature currents. Substituting Eq. (22) into Eq. (20), the total torque is expressed as:

$$k_\tau^T i_a = \tau_p - \tau_f \tag{23}$$

Furthermore, the joint effort caused by the end-effector contact with the environment is approximated based on Eq. (24) and the external force contact is estimated using Eq. (25).

$$\tau_f = \tau_p - k_\tau^T i_a \tag{24}$$

$$F = \left(J^T(\rho)\right)^\dagger \left(M(\rho)\ddot{\rho} + C(\rho, \dot{\rho})\dot{\rho} + D(\rho, \dot{\rho})\dot{\rho} + g(\rho) - k_\tau^T i_a\right) \tag{25}$$

3. The variable sliding mode dynamic controller

The structure proposed for motion and force control of the underwater manipulator is based on the parallel architecture presented in [32] and it is designed in the operational space. A separate control loop is designed for the position control law and a different control structure for the force regulation. The parallel control architecture aims to give priority to the force control loop in order to avoid large force interaction with the environment. The main contribution of the method presented here is the replacement of the proportional controllers used in the parallel structure from [32] with more robust architectures. Both the position and force control laws are part of the sliding mode controllers (SMC) and an approximation of the overall dynamic model of the robot is included in the final control law. An overall view of the control structure is presented in Fig. 1 and each component of the control law is next presented.

3.1. Position controller

The position control structure is represented based on the classic sliding mode controller and aims for the position error to converge to zero. The sliding mode variable δ is defined in Eq. (26)

$$\delta = \dot{e}_p + c_1 e_p, \quad c_1 > 0 \tag{26}$$

where $c_1 \in \mathbb{R}^{6\times6}$ is a positive matrix and $e_p = x_{des} - x$ represents the position error. To ensure that the position tracking error converges to zero, the following relationship has to be fulfilled:

$$\delta = \dot{e}_p + c_1 e_p = 0, \quad c_1 > 0 \tag{27}$$

The dynamics of the sliding mode variable is presented in Eq. (28) and is obtained by differentiating Eq. (26).

$$\dot{\delta} = \ddot{e}_p + c_1 \dot{e}_p, \quad c_1 > 0 \tag{28}$$

Substituting the dynamic model of the system, Eq. (1) into Eq. (28), the following expression is obtained:

$$\dot{\delta} = \ddot{x}_{des} - \ddot{x} + c_1 \dot{e}_p = \theta(x, \dot{x}, F) - M^{-1}(x)u_p \tag{29}$$

where $\mid \theta(x) \mid \leq \Omega_p$ is the bounded cumulative disturbance.

$$\begin{aligned}\theta(x) = \ddot{x}_{des} - M^{-1}(x)u_f - \\ - M^{-1}(x)\left[-F - C(x, \dot{x})\dot{x} - D(x, \dot{x})\dot{x} - G(x) - F_f(x)\right]\end{aligned} \tag{30}$$

The sliding mode existence condition, [33], for defining the control signal u_p fulfils the following requirement:

$$\delta\dot{\delta} \leq -\bar{\alpha} \mid \delta \mid, \quad \bar{\alpha} = \frac{\alpha}{\sqrt{2}}, \quad \alpha > 0 \tag{31}$$

$$\delta\dot{\delta} = \delta\left[\theta(x) - u_p\right] \leq \mid \delta \mid \Omega_p - \delta u_p \tag{32}$$

The control law is defined by Eq. (33). By incorporating this law into Eq. (32), the control gain can be tuned according to Eq. (35).

$$u_p = \kappa_1 \mathtt{sign}(\delta) \tag{33}$$

$$\delta\dot{\delta} \leq \mid \delta \mid (\Omega_p - \kappa_1) = -\bar{\alpha} \mid \delta \mid \tag{34}$$

$$\kappa_1 = \Omega_p + \bar{\alpha} \tag{35}$$

3.2. Force controller

The force controller aims to maintain the characteristics of the SMC controller but gives priority to the force control loop over the position controller. Based on this reasoning the Integral Sliding Mode Control (ISMC) theory, [34], is used to develop the force controller. The ISMC ensures the sliding mode behaviour from the start of the execution of the task. The structure consists of two components, a state feedback controller and a discontinuous controller, as presented by Eq. (36).

$$u_f = u_1 + u_2 \tag{36}$$

where $u_1 \in \mathbb{R}^6$, compensates for the bounded disturbances and $u_2 \in \mathbb{R}^6$ drives the sliding variable to zero in a finite time, taking into account that the sliding variable dynamics are no longer perturbed. The asymptotic stability of the system is provided by the feedback controller while the disturbances that might affect the system are handled by the discontinuous controller.

The primary sliding variable is represented by:

$$\sigma = \dot{e}_f + c_2 e_f + c_3 \int_0^t e_f d\tau, \quad c_2, c_3 > 0 \tag{37}$$

where e_f is the error in the end-effector force, $e_f = F_{des} - F$, defined based on the difference between the desired contact force $F_{des} \in \mathbb{R}^6$ and the current end-effector force $F \in \mathbb{R}^6$, $c_2 \in \mathbb{R}^{6\times6}$ and $c_3 \in \mathbb{R}^{6\times6}$ are positive constant diagonal matrices defined to model the sliding mode dynamics. The sliding variable dynamics is expressed by:

$$\dot{\sigma} = \ddot{e}_f + c_2 \dot{e}_f + c_3 e_f \tag{38}$$

The auxiliary sliding variable is designed by:

$$\begin{cases} s = \sigma - z \\ \dot{z} = -c_3 u_2 \end{cases} \tag{39}$$

The auxiliary sliding variable dynamics can be expressed by:

$$\begin{aligned}\dot{s} = \dot{\sigma} - \dot{z} = \ddot{e}_f + c_2 \dot{e}_f + c_3 e_f - (-c_3 u_2) = \\ = \ddot{e}_f + c_2 \dot{e}_f + c_3 (F_{des} - F) + c_3 u_2\end{aligned} \tag{40}$$

Substituting Eq. (16) into Eq. (41), the following expression is obtained:

$$\begin{aligned}\dot{s} = -c_3 u_1 - c_3 u_2 + \varphi(e_f, \dot{e}_f, u_p) + c_3 u_2 = \\ = -c_3 u_1 + \varphi(e_f, \dot{e}_f, u_p)\end{aligned} \tag{41}$$

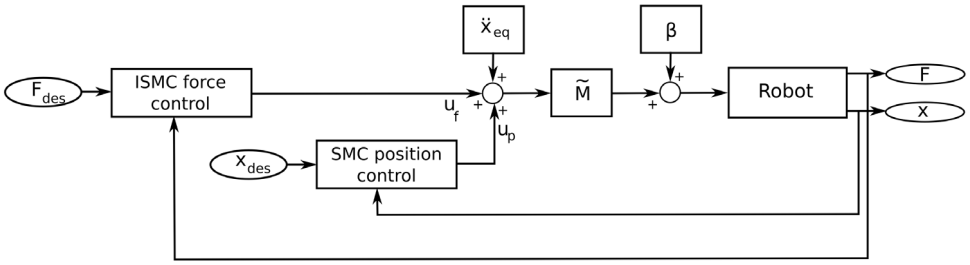

Fig. 1. Proposed control structure.

where

$$\begin{aligned}\varphi(e_f, \dot{e}_f, u_p) &= c_3\mu - c_3u_p + c_3F_{des} + c_2\dot{e}_f + \ddot{e}_f \\ \mu &= M(x)\ddot{x} + C(x,\dot{x})\dot{x} + D(x,\dot{x})\dot{x} + G(x) + F_f(x)\end{aligned} \tag{42}$$

and $|\ \varphi(e_f, \dot{e}_f, u_p)\ | \leq \Omega_f$ is the bounded disturbance term. To drive the sliding variable to zero in a finite time, the control command u_1 is defined by:

$$u_1 = \kappa_2 \mathtt{sign}(s) \tag{43}$$

Using the control law from Eq. (43) the sliding mode variable dynamics are expressed by Eq. (44).

$$\begin{cases}\dot{\sigma} = -c_3u_1 - c_3u_2 + \varphi(e_f, \dot{e}_f, u_p) \\ \dot{s} = -c_3u_1 + \varphi(e_f, \dot{e}_f, u_p), \quad u_1 = \kappa_2\mathtt{sign}(s)\end{cases} \tag{44}$$

By ensuring that $\dot{s} = 0$, the equivalent control u_{1eq} is defined by Eq. (45).

$$\begin{aligned}\dot{s} = 0 \Leftrightarrow &- c_3u_1 + \varphi(e_f, \dot{e}_f, u_p) = 0 \\ &\Rightarrow u_{1eq} = c_3^{-1}\varphi(e_p, \dot{e}_p, F)\end{aligned} \tag{45}$$

Substituting Eq. (45) into Eq. (44) the primary sliding mode variable dynamics is obtained. As can be seen from Eq. (46), the primary sliding mode is not dependent on the disturbances that have been removed by the secondary sliding mode function.

$$\dot{\sigma} = -c_3u_2 \tag{46}$$

In this case, to ensure asymptotic stability of the system, the primary control law u_2 can be formulated as:

$$u_2 = K\sigma, \quad K > 0 \tag{47}$$

where $K \in \mathbb{R}^{6\times6}$ is a positive matrix.

The chattering effect represents one of the disadvantages of the sliding mode controller. To reduce this effect, the `sign` function can be replaced by the `sigmoid` function expressed as:

$$\mathtt{sign}(a) \simeq \frac{a}{|\ a\ | + \epsilon} = \mathtt{sigmoid}(a) \tag{48}$$

where ϵ is a small positive scalar that has to be chosen in such a way that a smooth control action is ensured and satisfactory behaviour of the system is obtained.

3.3. Overall control structure

To remove the non-linearities a feedback linearisation technique is used in the final control law shown in Eq. (49).

$$\begin{aligned}T &= \tilde{M}(x)\left[\ddot{x}_{eq} + u_p + u_f\right] + \beta = \\ &= \tilde{M}(x)\left[\ddot{x}_{eq} + \kappa_1\mathtt{sigmoid}(\delta) + \kappa_2\mathtt{sigmoid}(s) + K\sigma\right] + \beta\end{aligned} \tag{49}$$

where

$$\begin{aligned}\delta &= \dot{e}_p + c_1e_p, \quad c_1 > 0 \\ \sigma &= \dot{e}_f + c_2e_f + c_3\int_0^t e_f d\tau, \quad c_2, c_3 > 0 \\ s &= \sigma - z \\ \dot{z} &= -c_3u_2 \\ u_2 &= K\sigma, \quad K > 0 \\ \beta &= \tilde{C}(x,\dot{x})\dot{x}_{eq} + \tilde{D}(x,\dot{x})\dot{x}_{eq} + \tilde{G}(x) + \tilde{F}_f(x) + \tilde{F}_{eq} \\ \dot{x}_{eq} &= \dot{x}_{des} + c_1e_p \\ F_{eq} &= F_{des} + c_2^{-1}\dot{e}_f + c_2^{-1}c_3\int_0^t e_f d\tau\end{aligned} \tag{50}$$

$\tilde{M}(x)$ is an estimate of the inertia term, $\tilde{C}(x,\dot{x})$, $\tilde{D}(x,\dot{x})$, $\tilde{G}(x)$, $\tilde{F}_f(x)$ are estimates of the real values of the system defined in operational space coordinates according to the boundary errors, $\delta M(x)$, $\delta C(x,\dot{x})$, $\delta D(x,\dot{x})$, $\delta G(x)$ and $\delta F_f(x)$ by Eq. (51).

$$\begin{aligned}|\ \Delta M(x)\ | &\leq \delta M(x) \quad \Delta M(x) = M(x) - \tilde{M}(x) \\ |\ \Delta C(x,\dot{x})\ | &\leq \delta C(x,\dot{x}) \quad \Delta C(x,\dot{x}) = C(x,\dot{x}) - \tilde{C}(x,\dot{x}) \\ |\ \delta D(x,\dot{x})\ | &\leq \delta D(x,\dot{x}) \quad \Delta D(x,\dot{x}) = D(x,\dot{x}) - \tilde{D}(x,\dot{x}) \\ |\ \Delta G(x)\ | &\leq \delta G(x) \quad \Delta G(x) = G(x) - \tilde{G}(x) \\ |\ \Delta F_f(x)\ | &\leq \delta F_f(x) \quad \Delta F_f(x) = F_f(x) - \tilde{F}_f(x)\end{aligned} \tag{51}$$

To summarise, the proposed control structure is characterised by the following components and their roles:

- Model linearisation: to decouple the system.
- Parallel position/force structure: simultaneous control of the position and force behaviour of the system.
- Position control law, u_p: sliding mode control to ensure trajectory tracking in the presence of hydrodynamic disturbances, unknown model parameters and significant coupling effects between the manipulator and vehicle.
- Force control law, u_f: integral sliding mode control to ensure zero force error and gives priority to the force component over the position component.

The control parameters are selected based on trial and error and in such a way to obtain a reliable compromise between the interaction and tracking behaviour of the end effector.

3.4. Lyapunov stability analysis

Using the mathematical model of the manipulator in the operational space described by Eq. (16) and the total control law defined in Eq. (50), the closed-loop system is described by:

$$\begin{aligned}&M(x)\ddot{x} + C(x)\dot{x} + D(x)\dot{x} + G(x) + F_f(x) = \\ &= \tilde{M}(x)\left[\ddot{x}_{eq} + \kappa_1\mathtt{sign}(\delta) + \kappa_2\mathtt{sign}(s) + K\sigma\right] + \\ &+ \tilde{C}(x,\dot{x})\dot{x}_{eq} + \tilde{D}(x,\dot{x})\dot{x}_{eq} + \tilde{G}(x) + \tilde{F}_f(x) + \tilde{F}_{eq} - F\end{aligned} \tag{52}$$

For simplicity, the dynamic model parameters $M(x)$, $C(x)\dot{x}$, $D(x)\dot{x}$, $G(x)$, $F_f(x)$ are denoted as M, C, D, G, F_f. We define a new variable $\dot{\delta}$ as $\dot{\delta} = \dot{x}_{eq} - \dot{x}$. Using this relation to substitute $\ddot{x}$ by $\ddot{x} = \ddot{x}_{eq} - \dot{\delta}$ in Eq. (52) the closed-loop system can be expressed as:

$$\begin{aligned} M\ddot{\delta} = &-\tilde{M}\ddot{x}_{eq} - \tilde{M}\kappa_1 \mathtt{sign}(\delta) - \tilde{M}\kappa_2 \mathtt{sign}(s) - \tilde{M}K\sigma + \\ &+ F_{eq} - c_2^{-1}\sigma - -\tilde{C}\dot{x}_{eq} - \tilde{D}\dot{x}_{eq} - \tilde{G} - \tilde{F}_f - \tilde{F}_{eq} + \\ &+ M\ddot{x}_{eq} + C\dot{x}_{eq} + D\dot{x}_{eq} + G + F_f - C\delta - D\delta \end{aligned} \tag{53}$$

Using the boundary errors from Eq. (51), Eq. (53) can be expressed as:

$$\begin{aligned} M\ddot{\delta} = &-\tilde{M}\kappa_1 \mathtt{sign}(\delta) - \tilde{M}\kappa_2 \mathtt{sign}(s) - \tilde{M}K\sigma - \\ &- c_2^{-1}\sigma - C\delta - D\delta + \Delta M\ddot{x}_{eq} + \Delta C\dot{x}_{eq} + \\ &+ \Delta D\dot{x}_{eq} + \Delta G + \Delta F_f + \Delta F_{eq} \end{aligned} \tag{54}$$

Defining the Lyapunov function candidate as:

$$V = \frac{1}{2}\delta^T M\delta \tag{55}$$

As $\delta^T M\delta$ is a positive term, the Lyapunov function candidate is positive. The derivative of V is given by:

$$\dot{V} = \frac{1}{2}\delta^T \dot{M}\delta + \delta^T M\dot{\delta} \tag{56}$$

Replacing $M\dot{\delta}$ with the expression from Eq. (54), Eq. (56) becomes:

$$\begin{aligned} \dot{V} = &\delta^T \left[-\tilde{M}\kappa_1 \mathtt{sign}(\delta) - \tilde{M}\kappa_2 \mathtt{sign}(s)\right] + \\ &+ \delta^T \left[-\tilde{M}K\sigma - c_2^{-1}\sigma - C\delta - D\delta\right] + \frac{1}{2}\delta^T \dot{M}\delta + \\ &+ \delta^T \left[\Delta M\ddot{x}_{eq} + \Delta C\dot{x}_{eq} + \Delta D\dot{x}_{eq} + \Delta G + \Delta F_f + \Delta F_{eq}\right] \end{aligned} \tag{57}$$

To simplify the expression of $\dot{V}$ the following notations are made which define positive matrices:

$$\Lambda_1 = \tilde{M}\kappa_1 \quad \Lambda_2 = \tilde{M}\kappa_2 \quad \Lambda_3 = \tilde{M}K + c_2^{-1}$$

and

$$S = \mathtt{sign}(s)$$

Eq. (57) can be now expressed as:

$$\begin{aligned} \dot{V} = &-\delta^T \Lambda_1 \mathtt{sign}(\delta) - \delta^T \Lambda_2 S - \delta^T \Lambda_3 \sigma + \\ &+\delta^T \left[\Delta M\ddot{x}_{eq} + \Delta C\dot{x}_{eq} + \Delta D\dot{x}_{eq} + \Delta G +\right] + \\ &+\delta^T \left[\Delta F_f + \Delta F_{eq}\right] + \delta^T \left[\frac{1}{2}\dot{M}\delta - C\right]\delta - \delta^T D\delta \end{aligned} \tag{58}$$

From Eq. (58) it can be seen that the derivative of the Lyapunov function can be bounded by the following expression:

$$\begin{aligned} \dot{V} \leq &-\delta^T D\delta + \delta^T \left[\Delta M\ddot{x}_{eq} + \Delta C\dot{x}_{eq} + \Delta D\dot{x}_{eq} + \Delta G +\right] + \\ &+\delta^T \left[\Delta F_f + \Delta F_{eq}\right] - \delta^T \Lambda_1 \mathtt{sign}(\delta) - \frac{a_1}{2}\delta^T \Lambda_2 \delta - \\ &- \frac{1}{2a_1} S^T \Lambda_2 S - \frac{a_2}{2}\delta \Lambda_3 \delta - \frac{1}{2a_2}\sigma \Lambda_3 \sigma \end{aligned} \tag{59}$$

where a_1, a_2 are positive constants. By choosing:

$$\begin{aligned} \lambda_i \geqslant &\mid \left[\Delta M\ddot{x}_{eq} + \Delta C\dot{x}_{eq} + \Delta D\dot{x}_{eq} +\right]_i \mid + \\ &+ \mid \left[\Delta G + \Delta F_f + \Delta F_{eq}\right]_i \mid + \eta_i \end{aligned} \tag{60}$$

where η_i is positive, $i = 1, \ldots, 6$ and $[..]_i$ represents the ith element of the array computed between the brackets. Then:

$$\begin{aligned} \dot{V} \leq &-\bar{\lambda}_D \|\delta\|^2 - \sum_{i=1}^{6} \eta_i \mid \lambda_i \mid - \frac{a_1}{2}\bar{\lambda}_2 \|\delta\|^2 - \\ &- \frac{1}{2a_1}\bar{\lambda}_2 \|s\|^2 - \frac{a_2}{2}\bar{\lambda}_3 \|\delta\|^2 - \frac{1}{2a_2}\bar{\lambda}_3 \|\sigma\|^2 \end{aligned} \tag{61}$$

where $\bar{\lambda}_D$ is the largest eigenvalue of D, λ_i is defined according to Eq. (60) and $\bar{\lambda}_2$, $\bar{\lambda}_3$ are the largest eigenvalues of Λ_2, Λ_3. As the function V is a positive definite function and $\dot{V}$ is a negative definite function, for the UVMS defined by Eq. (1) and controlled by Eq. (49) the sliding mode is guaranteed and the errors converge to zero.

4. Experimental set-up

The experimental results are obtained using the 6 degrees-of-freedom underwater manipulator HDT-MK3-M available in the Ocean Systems Laboratory. The manipulator has absolute position sensors and current sensors at each joint. The maximum joint speed is 0.7 rad/s (equivalent of 40 deg/s) and the maximum joint torque is 60 Nm for every joint of the arm. A detailed description of the manipulator parameters can be seen in Table 1. The weight in air of the arm is 9 kg while in water it has a weight of 3 kg. The arm does not have an end-effector force sensor that can be used to measure the interaction force with the environment.

The manipulator is mounted on the Integration Kit that is attached to a fixed base and placed in an indoor tank. The base of the manipulator is placed at 0.2 m underwater. The Integration Kit is responsible for the communication between the exterior world and the drives of the arm and incorporates the power electronics of the system.

Two different set-ups for interacting with the environment are used: one represented by a plastic ball submerged and the other scenario consisting of an aluminium plate submerged. The two cases can be seen in Fig. 2. In both cases the object is placed in the work-space of the manipulator. The desired goal where the end-effector is requested to reach is represented by the central position of the object. The desired interaction force with the environment is requested in the neighbourhood of the final goal, based on a tolerance margin. As soon as the end-effector is outside of this tolerance boundary, the applied force to the object should be zero.

The stiffness coefficients for the two objects used in this experimental set-up are computed based on a simple point model. It is out of the scope of this study to accurately calculate these coefficients, the interest being on the order of the coefficients which can be obtained based on Eq. (62).

$$K_e = \frac{EA}{L} \tag{62}$$

where L is the length of the object, A is the cross-sectional area and E is the Young's modulus. Using the elasticity coefficients as presented in [35] and based on the dimensions of the two objects used for these experiments, for the plastic ball, the stiffness coefficient is approximately $K_e = 1.75 \times 10^8$ Nm and for the aluminium plate the coefficient is $K_e = 3.3 \times 10^{11}$ Nm.

The controllers are implemented in Python on an external computer. The torque required for the end-effector to move is sent to the drives of the manipulator arm, bypassing the existing joint controllers of the arm. The drives provide the current joint position and velocity. The communication takes place at a frequency of 10 Hz representing the arm's maximum frequency. The kinematic model of the arm and the waypoints the end-effector has to follow to reach the final goal are computed using the `ROS-MoveIT`[36] software. The path generated represents the optimal path and takes into consideration the joint limits and self-collision information. By using this method to generate the trajectory, it is ensured that the arm is not put into a singular configuration. As a safety feature the maximum current drawn by each motor is limited to 3 A.

Table 1
Manipulator joint parameters.

Joint	Min joint (rad)	Max joint (rad)	Max velocity (rad/s)	Max torque (Nm)	Max current (A)
Shoulder roll	−3.14	3.14	0.7	60	8
Shoulder pitch	−1.57	3.14	0.7	60	8
Elbow pitch	−1.57	3.14	0.7	60	8
Wrist roll	−3.14	3.14	0.7	60	8
Wrist yaw	−1.57	1.57	0.7	60	8
Wrist pitch	−1.57	1.57	0.7	60	8

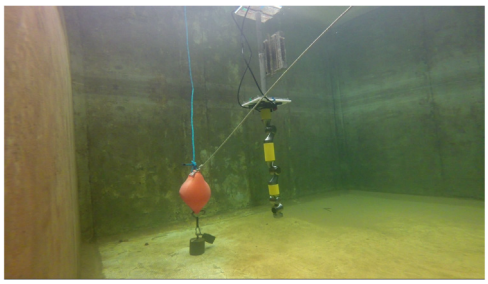

(a) Plastic ball.

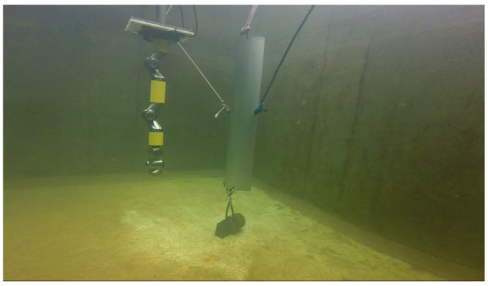

(b) Aluminium plate.

Fig. 2. Experimental set-up.

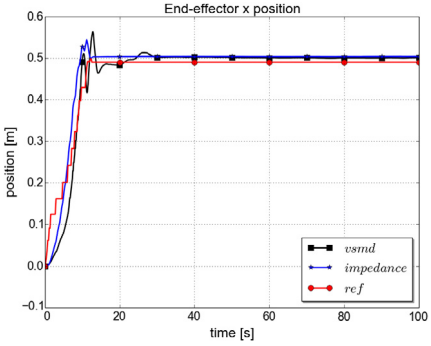

(a) x-axis trajectory.

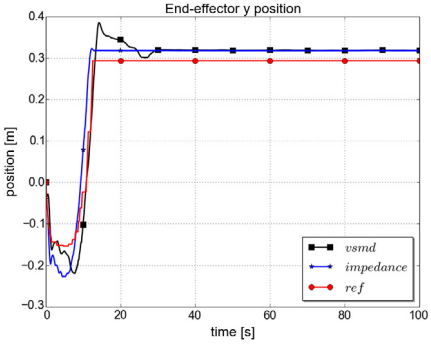

(b) y-axis trajectory.

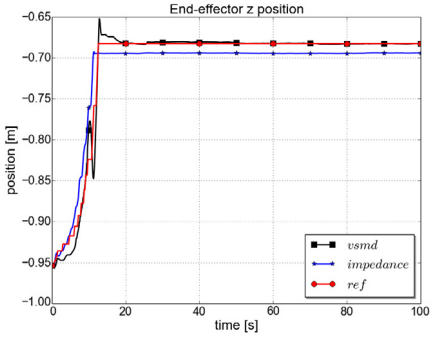

(c) z-axis trajectory.

Fig. 3. End-effector trajectory tracking (contact with a plastic ball).

5. Experimental results

The experimental results present a comparison between the proposed VSMD controller and the Impedance controller as described in [37]. The world coordinates are defined at the base of the manipulator coinciding with the base coordinates of the arm. An assumption is made that the contact with the environment takes place principally on the x-axis of the object coordinates which coincides with the x-axis of the world coordinates. The end-effector force contact estimated on the x-axis as a point-contact is considered in this paper. As presented in [38] in the case when orientation control is incorporated into the system the performance of the task space position tracking deteriorates compared with the case when orientation constraints are not included into the system. This is caused due to the reduction of the redundancy of the system and represents the reason that led to control only the position tracking of the end-effector and not incorporating any constraints on the orientation of the end-effector. To compute the end-effector trajectory the joint positions and the kinematic model of the arm is used. Using the CAD files provided by the manufacturer of the arm, the Kinematics and Dynamics Library (KDL) [39] is used to compute the forward kinematics of the arm. In the experiments presented in this paper the end-effector force is computed using the mathematical model of the robot and considering the torque-current relationship. Details of the method have been presented in Section 2.

5.1. Interaction with a plastic ball

The first group of experiments represents the interaction of the end-effector of the manipulator arm with a submerged plastic ball. The ball (the desired goal) is located at $(0.5,\ 0.3,\ -0.7)$ m in the world coordinates. The task is that the end-effector has to follow the optimal trajectory generated by the `MoveIt` software until it reaches the ball. At the moment the end-effector reaches the vicinity of the goal, the manipulator should apply a contact force on the object of $F_{des} = 100$ N. The vicinity of the goal is dependent of the diameter of the ball, in this case it is 0.3 m.

In Fig. 3 the behaviour of the x, y and z axes is presented for the Impedance controller and for the VSMD controller. The end-effector behaviour using the two controllers is similar, reaching the steady-state in less than 15 s. A small steady-state error is observed for the x and y axes, Figs. 3(a) and 3(b), for both controllers. For the z axis, the steady-state error is eliminated when using the VSMD, while using the Impedance controller there is an offset between the desired value and the real z axis value. The VSMD enforces one of the axes to reach zero steady-state error but this leads to an overshoot in all axes when this controller is used.

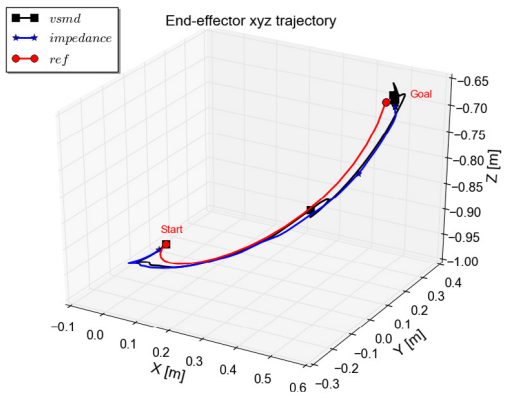

Fig. 4. End-effector 3D trajectory, contact with a plastic ball.

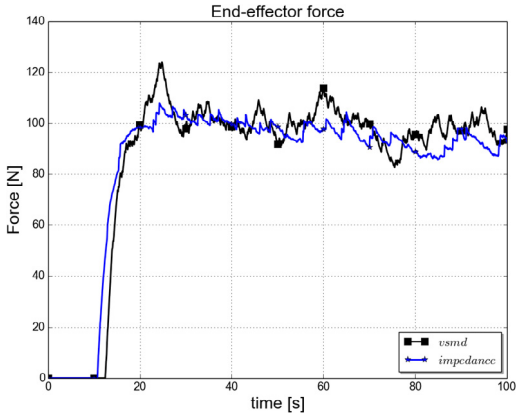

Fig. 5. Interaction with a plastic ball.

The 3D behaviour of the end-effector is seen in Fig. 4. The end-effector initial location is at $(0,\ 0,\ -0.97)$ m. As mentioned previously, the end-effector behaviour using the two controllers is similar, both have a small offset from the desired trajectory.

The interaction with the environment is presented in Fig. 5. The behaviour of the contact force is more oscillatory when the VSMD controller is used compared to the case when the Impedance controller is used. The VSMD controller is characterised by two control loops acting in parallel. Although the force loop has priority over the position control loop, the latter one is still active at the same time as the force one. In this case the force controller is responsible for reaching and maintaining the desired force while the position controller is responsible for reaching the desired location. Both the Impedance and VSMD controllers maintain appropriate force contact with the ball.

5.2. Interaction with an aluminium plate

The performances of the controller are evaluated using an aluminium plate with a width of 0.4 m and a height of 1 m, placed at different locations in the workspace. The final goal of the end-effector is described as a point on the plate, placed at $(-0.22,\ -0.22,\ -0.8)$ m in the world coordinates. The allowed vicinity of this point where the end-effector should apply a contact force of $F_{des} = 10$ N is described by a circle with a radius of 0.3 m.

In Fig. 6 the independent behaviour in the x, y and z axes is presented. The configuration of the arm to reach this end-effector goal is more challenging than the previous case. The Impedance controller performance is degraded for this goal and this type of environment. A small displacement is seen on the x and y axes that does not significantly affect the behaviour of the system. Nevertheless, the displacement on the z axis is 0.1 m. The desired location is reached when the VSMD controller is used, although the settling time is 60 s and it presents an oscillatory behaviour. The path the end-effector takes to reach the goal is presented in Fig. 7.

Due to noisy current sensor readings the interaction force with the environment shown in Fig. 8 is also noisy. For the aluminium plate, the desired interaction with the environment is lower to remove the possibility of damaging the arm. An overshoot is present in the force response when using the VSMD controller caused by the two components of the controller working in parallel. As the desired position goal is achieved the desired contact force is also met. An offset in the interaction force with the environment is present when the impedance controller is used. This is related to the position error, Fig. 6(a), as the force is controlled through the location of the end-effector.

6. Discussion

The behaviour of the HDT-MK3-M manipulator when using the two controllers is evaluated based on the generalised root mean-square error (GRMS), the peak tracking error and the lowest tracking error. The test set consists of 20 different end-effector goals. For 10 of these goals the interaction is with the plastic ball while for the other 10 the interaction with the aluminium plate is the goal. A range of contact forces are used for these experiments, from 1 N up to 100 N.

The results are presented in Table 2 and are divided accordingly into position errors and force errors. The peak position tracking error is obtained using the Impedance controller while the lowest position tracking error has the same value using either of the two controllers. The difference between the lowest position error and the peak position error is largest for the Impedance controller. Nevertheless, the GRMS position error has similar values using either of the two controllers. In the case of the force errors, the GRMS error is higher for the Impedance controller compared with the VSMD controller. A significant difference between the peak force error and the lowest force error is observed for both controllers. This is due to the overshoot present using the VSMD controller and the constant offset in the force response when the Impedance controller is used.

Based on the simulation results and the tracking errors it can be stated that the proposed VSMD controller has a similar performance to the Impedance controller. Accurate force tracking is difficult as an end-effector sensor is not available. The noisy available sensor measurements and the use of the Jacobian matrix to compute the end-effector force can be a source of disturbance for the force control loop. It was noticed that using different types of environments does not highly influence the behaviour of the controller. In the case of the aluminium plate, it was desired to have lower interaction forces as a safety measure. The aluminium plate represents a hard environment and interacting at high forces might damage the robotic arm, especially if there is a large overshoot in the force response.

The method proposed in this paper can be compared with the method recently developed by [21]. The similarity of the two methods rests in the fact that both methods use sliding mode controllers and both aim in obtaining a smooth behaviour when passing from position to force tracking. While in [21] this is achieved modifying the selection matrix in the hybrid strategy, in this paper a smooth behaviour is obtained by giving different priorities to the two components of the controller. Furthermore, a task controller in operational space designed based simply on an integrals sliding mode controller is presented in [40]. Similar to our approach the method aims to obtain a force/position tracking but instead of

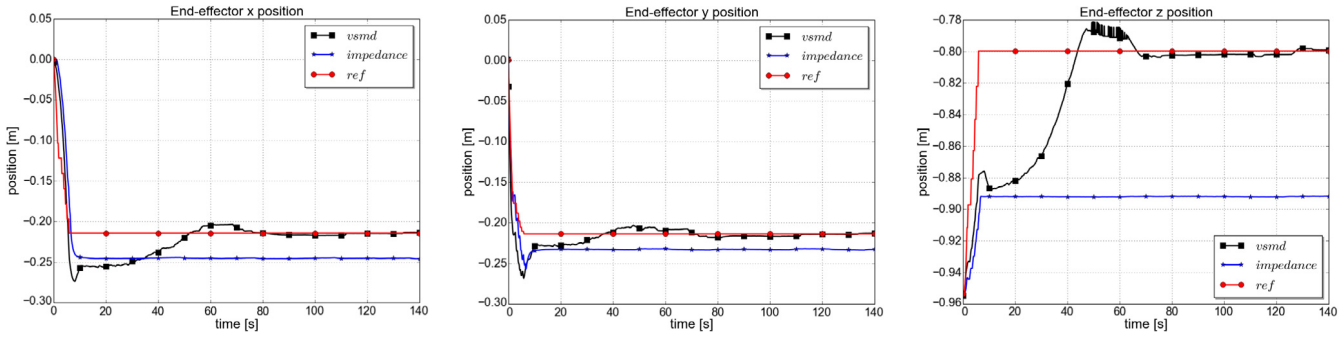

(a) x-axis trajectory. (b) y-axis trajectory. (c) z-axis trajectory.

Fig. 6. End-effector trajectory tracking (contact with an aluminium plate).

Table 2
Performance errors for position/force control of manipulator.

Method	Position errors			Force errors		
	e_{GRMS} (m)	e_{peak} (m)	e_{low} (m)	e_{GRMS} (N)	e_{peak} (N)	e_{low} (N)
Impedance	0.06	0.1	0.04	2.58	4.02	0.76
VSMD	0.05	0.06	0.04	2.08	3.26	1.33

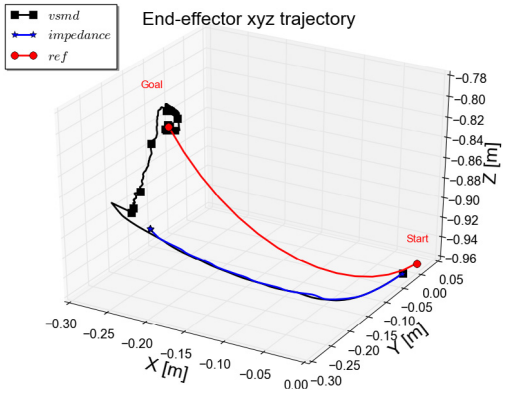

Fig. 7. End-effector 3D trajectory (contact with an aluminium plate).

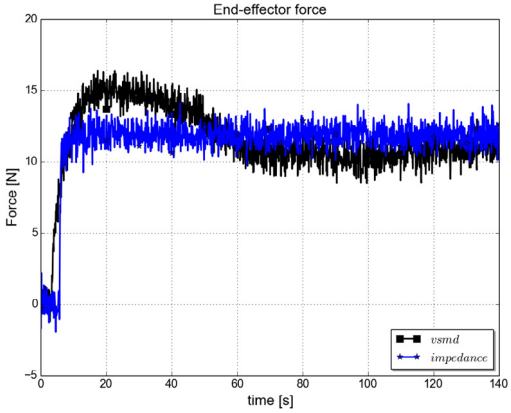

Fig. 8. Interaction with an aluminium plate.

using two SMC strategies a single ISMC controller is used that imposes virtual mass–spring–damper behaviour achieving complaint trajectory tracking. Nevertheless, it can be seen from the results that accurate force tracking is difficult to maintain using either of the methods.

During the experimental testing, it was observed that tuning the operational-space controllers can be challenging. The controller output is mapped from operational space to joint space, making the current commands sent to the joints dependent on the arm configuration. In this case, although the tuning of the parameters at end-effector level is appropriate and there is an optimal path generated previously, transforming the control effort from the operational space to joint level might lead to an overshoot in the system response or not achieving zero steady-state error.

7. Conclusions

In this paper the structure of the Variable Structure Model Dynamic Controller for an underwater manipulator performing motion and interaction tasks is introduced for the first time. The mathematical structure of the controller incorporates the parallel position/force controller, the sliding mode theory and the mathematical model of the robot. The proposed control strategy represents a robust architecture that is able to handle the nonlinear underwater system and the effects of the interaction with the environment. The controller is compared to the Impedance controller using an experimental set-up comprised of an underwater manipulator placed at a depth of 0.5 m in an underwater tank. The experimental results show that the VSMD controller produces comparable results to the Impedance controller for both position and force tracking. The interaction force between the end-effector and the environment is approximated based on the joint sensor information and the manipulator Jacobian. Using appropriate trajectory generation for the end-effector, the desired goal is reached and the contact with the environment is maintained.

Acknowledgements

The authors would like to acknowledge the financial support provided by the ETP program Scotland and SeeByte Ltd.

References

[1] Z.H. Ismail, Task-space dynamic control of underwater robots, (Ph.D. thesis), Heriot-Watt University, UK, 2011.
[2] O. Khatib, Y. Yokoi, K. Chang, R. Ruspini, R. Holmberg, A. Casal, Vehicle/arm coordination and multiple mobile manipulator decentralized cooperation, in: Proceedings of the IEEE/RSJ International Conference on Intelligent Robots and Systems, 2, 1996, pp. 546–553.

[3] C. Tang, Y. Wang, S. Wang, M. Tan, Robust iterative multi-task control of the underwater biomimetic vehicle-manipulator system, in: IEEE International Conference on Robotics and Biomimetics, ROBIO, 2016, pp. 823–828.
[4] Q. Tang, L. Liang, J. Xie, Y. Li, Z. Deng, Task-priority redundancy resolution on acceleration level for underwater vehicle-manipulator system, Int. J. Adv. Robot. Syst. 14 (2017).
[5] E. Cataldi, G. Antonelli, Basic interaction operations for an underwater vehicle-manipulator system, in: 2015 International Conference on Advanced Robotics, ICAR, 2015, pp. 524–529.
[6] J.I. Kang, H.S. Choi, B.H. Jun, N.D. Nguyen, J.Y. Kim, Control and implementation of underwater vehicle manipulator system using zero moment point, in: IEEE Underwater Technology, UT, 2017, pp. 1–5.
[7] P.S. Londhe, M. Santhakumar, B.M. Patre, L.M. Waghmare, Task space control of an autonomous underwater vehicle manipulator system by robust single-input fuzzy logic control scheme, IEEE J. Ocean. Eng. 42 (2017) 13–28.
[8] O. Kermorgant, Y. Petillot, M.W. Dunnigan, A global control scheme for free-floating vehicle-manipulators, in: 2013 IEEE/RSJ International Conference on Intelligent Robots and Systems, 2013, pp. 5015–5020.
[9] D.R. Yoerger, H. Schempf, D.M. DiPietro, Design and performance evaluation of an actively compliant underwater manipulator for full-ocean depth, J. Robot. Syst. 8 (1991) 371–392.
[10] M.W. Dunnigan, D.M. Lane, A.C. Clegg, I. Edwards, Hybrid position/force control of a hydraulic underwater manipulator, IEE Proc. - Control Theory Appl. 143 (1996) 145–151.
[11] G. Antonelli, N. Sarkar, S. Chiaverini, Explicit force control for underwater vehicle-manipulator systems, Robotica 20 (2002) 251–260.
[12] Y. Cui, N. Sarkar, A unified force control approach to autonomous underwater manipulation, Robotica 19 (2001) 255–266.
[13] S. Heshmati-alamdari, A. Nikou, K.J. Kyriakopoulos, D.V. Dimarogonas, A robust control approach for underwater vehicle manipulator systems in interaction with compliant environments, arXiv preprint arXiv:1611.07399, 2016.
[14] T.W. McLain, S.M. Rock, M.J. Lee, Experiments in the coordination of underwater manipulator and vehicle control, in: MTS/IEEE Oceans, Vol. 2, 1995, pp. 1208–1215.
[15] B. Xu, S.R. Pandian, M. Inoue, N. Sakagami, S. Kawamura, et al., Model-based sliding mode control of underwater robot manipulators, Int. J. Offshore Polar Eng. 16 (2006).
[16] H.N. Esfahani, V. Azimirad, A new fuzzy sliding mode controller with pid sliding surface for underwater manipulators, Int. J. Mechatron. Electr. Comput. Technol. 3 (2013) 224–249.
[17] B. Xu, S.R. Pandian, F. Petry, A sliding mode fuzzy controller for underwater vehicle-manipulator systems, in: Annual Meeting of the North American Fuzzy Information Processing Society, NAFIPS, 2005, pp. 181–186.
[18] G. Bartolini, M. Coccoli, E. Punta, Sliding mode control of an underwater robotic manipulator, in: IEEE Conference on Decision and Control, Vol. 3, 2000, pp. 2983–2988.
[19] C.D. Onal, K. Abidi, A. Sabanovic, A cascaded sliding mode hybrid force/position controller, in: Proceedings of the IEEE International Symposium on Industrial Electronics, 2005. ISIE 2005. Vol. 1, 2005, pp. 183–188.
[20] E.D. Engeberg, S.G. Meek, M.A. Minor, Hybrid force–velocity sliding mode control of a prosthetic hand, IEEE Trans. Biomed. Eng. 55 (2008) 1572–1581.
[21] J. Wu, S. Fan, S. Shi, Z. Li, M. Jin, H. Liu, Sliding mode hybrid impedance control of manipulators for complex interaction tasks, in: 2017 IEEE International Conference on Advanced Intelligent Mechatronics, AIM, 2017, pp. 1009–1014.
[22] A. Hace, S. Uran, K. Jezernik, B. Curk, Robust sliding mode based impedance control, in: Proceedings of IEEE International Conference on Intelligent Engineering Systems, 1997, pp. 77–82.
[23] R. Featherstone, Rigid Body Dynamics Algorithms, Springer-Verlag New York Inc., 2007.
[24] G.E. Owen, Fundamentals of Scientific Mathematics, Courier Corporation, 2003.
[25] J. Newman, Marine Hydrodynamics, MIT Press, Cambridge, MA, 1989.
[26] M. Hosseini, A. Omidi, O. Meghdari, G. Vossoughi, A composite rigid body algorithm for modeling and simulation of an underwater vehicle equipped with manipulator arms, J. Offshore Mech. Arctic Eng. 128 (2005) 119–132.
[27] O. Khatib, A unified approach for motion and force control of robot manipulators: The operational space formulation, IEEE J. Robot. Automat. 3 (1987) 43–53.
[28] O. Khatib, Motion/force redundancy of manipulators, in: USA Symposium on Flexible Automation, Vol. 23, 1990, pp. 337–342.
[29] A. Stolt, On Robotic Assembly using Contact Force Control and Estimation, Lund University, 2015.
[30] M. Van Damme, P. Beyl, B. Vanderborght, V. Grosu, R. Van Ham, I. Vanderniepen, A. Matthys, D. Lefeber, Estimating robot end-effector force from noisy actuator torque measurements, in: IEEE International Conference on Robotics and Automation, ICRA, IEEE, 2011, pp. 1108–1113.
[31] K.S. Eom, I.H. Suh, W.K. Chung, S.-R. Oh, Disturbance observer based force control of robot manipulator without force sensor, in: International Conference on Robotics and Automation, ICRA, Vol. 4, 1998, pp. 3012–3017.
[32] S. Chiaverini, L. Sciavicco, The parallel approach to force/position control of robotic manipulators, IEEE Trans. Robot. Autom. 9 (1993) 361–373.
[33] Y. Shtessel, C. Edwards, L. Fridman, A. Levant, Sliding Mode Control and Observation, Springer, 2014.
[34] V. Utkin, J. Shi, Integral sliding mode in systems operating under uncertainty conditions, in: Proceedings of the 35th IEEE Conference on Decision and Control, Vol. 4, 1996, pp. 4591–4596.
[35] E.R. Parker, Materials Data Book for Engineers and Scientists, 1967.
[36] MoveIT, http://moveit.ros.org/, 2017.
[37] S.I. Part, Impedance control: An approach to manipulation, J. Dynam. Syst. Meas. Control 107 (1985) 17.
[38] J. Nakanishi, R. Cory, M. Mistry, J. Peters, S. Schaal, Operationl space control: A theoretical and empirical comparison, Int. J. Robot. Res. 27 (2008) 737–757.
[39] Kinematics, D. Lybrary, http://www.orocos.org/kdl, 2017.
[40] G. Herrmann, J. Jalani, M.N. Mahyuddin, S.G. Khan, C. Melhuish, Robotic hand posture and compliant grasping control using operational space and integral sliding mode control, Robotica 34 (2016) 2163–2185.

Corina Barbalata is currently a research fellow in the Deep Robot Optical Perception (DROP) Laboratory from the Naval Architecture and Marine Engineering Faculty at University of Michigan. In 2017 she received a Ph.D. in Electrical Engineering from Heriot-Watt University UK, in 2013 she got her M.Sc. from University of Burgundy in France and previously she graduated in 2011 with a B.Sc. from Transilvania University in Romania. Her research interests include low-level control systems and motion planning algorithms, focusing on underwater robotic systems and mobile manipulation. She is interested in coupled control of lightweight systems and energy efficient control methods.

Matthew W. Dunnigan received his B.Sc. in Electrical and Electronic Engineering (with First-Class Honours) from Glasgow University, Glasgow, UK, in 1985 and his M.Sc. and Ph.D. from Heriot-Watt University, Edinburgh, UK, in 1989 and 1994, respectively. He was employed by Ferranti from 1985 to 1988 as a Development Engineer in the design of power supplies and control systems for moving optical assemblies and device temperature stabilisation. In 1989, he became a Lecturer at Heriot-Watt University, where he was concerned with the evaluation and reduction of the dynamic coupling between a robotic manipulator and an underwater vehicle. He is currently Associate Professor and his research grants and interests include the areas of hybrid position/force control of an underwater manipulator, coupled control of manipulator-vehicle systems, nonlinear position/speed control and parameter estimation methods in vector control of induction machines, frequency domain selftuning/ adaptive filter control methods for random vibration, and shock testing using electrodynamic actuators.

Yvan Petillot is a Professor of Robotics and Computer Vision at Heriot-Watt University. He is a leading member of the Oceans Systems Laboratory, the deputy director of the Institute for Sensor Signals and Systems and the deputy director of the joint research institute in Signal and Image Processing (ERP-SIP) with Edinburgh University. Yvan specialises in robotics and sensing and is an expert in autonomous systems, image analysis and control applied to the subsea domain. He has made major contributions in sonar image processing and target detection and recognition.